Meccanica

'Explicit' and 'implicit' non-local continuous descriptions for a circular plate with an inclusion in tension

--Manuscript Draft--

Manuscript Number:	
Full Title:	'Explicit' and 'implicit' non-local continuous descriptions for a circular plate with an inclusion in tension
Article Type:	S.I. : Computational Models for 'Complex' Materials and Structures
Section/Category:	Solids
Keywords:	Non-local models; Cosserat; Eringen; nonhomogeneous solids; finite elements; scale effects
Corresponding Author:	Meral TUNA EROGLU, M.Sc Istanbul Teknik Universitesi Istanbul, TURKEY
Corresponding Author Secondary Information:	
Corresponding Author's Institution:	Istanbul Teknik Universitesi
Corresponding Author's Secondary Institution:	
First Author:	Meral TUNA EROGLU, M.Sc
First Author Secondary Information:	
Order of Authors:	Meral TUNA EROGLU, M.Sc
	Lorenzo Leonetti, Ph. D.
	Patrizia Trovalusci, Ph. D.
	Mesut Kirca, Ph. D.
Order of Authors Secondary Information:	
Funding Information:	Ministero dell'Istruzione, dell'Università e della Ricerca (B86J16002300001) — Mrs. Meral TUNA EROGLU
Abstract:	Increasing application of composite structures in engineering field inherently speed up the studies focusing on the investigation of non-homogeneous bodies. Due to their capability on capturing the size effects, and offering solutions independent of spatial discretization, enriched non-classical continuum theories are often more preferable with respect to the classical ones. In the present study, the sample problem of a plate with a circular inclusion subjected to a uniform tensile stress is investigated in terms of both 'implicit'/'weak' and 'explicit'/'strong' non-local descriptions: Cosserat (micropolar) and Eringen theories, by employing the finite element method. The material parameters of 'implicit' model is assumed to be known, while the nonlocality of 'explicit' model is optimized according to stress concentration factors reported for infinite Cosserat plates. The advantages/disadvantages, and correspondence/non-correspondence between both non-local models are highlighted and discussed apparently for the first time, by comparing the stress field provided for reference benchmark problem under various scale ratios, and material parameter combinations for matrix-inclusion pair. The results reveal the analogous character of both non-local models in case of geometric singularities, which may pave the way for further studies considering problems with noticeable scale effects and load singularities.

'Explicit' and 'implicit' non-local continuous descriptions for a circular plate with an inclusion in tension

†Meral Tuna, Lorenzo Leonetti, Patrizia Trovalusci, Mesut Kirca

†M. Tuna
Ph.D. Candidate, M.Sc.
Department of Mechanical Engineering,
Istanbul Technical University, Istanbul, Turkey
e-mail: tunamer@itu.edu.tr

L. Leonetti
Research fellow, Ph.D.
Department of Structural Engineering,
University of Calabria, Rende, Italy
e-mail: lorenzo.leonetti@unical.it

P. Trovalusci
Full Professor of Solids and Structural Mechanics, Ph.D.
Department of Structural and Geotechnical Engineering,
Sapienza - University of Rome, Rome, Italy
e-mail: patrizia.trovalusci@uniroma1.it

M. Kirca
Associated Professor, Ph.D.
Department of Mechanical Engineering,
Istanbul Technical University, Istanbul, Turkey
e-mail: kircam@itu.edu.tr

†Corresponding author

Abstract

Increasing application of composite structures in engineering field inherently speed up the studies focusing on the investigation of non-homogeneous bodies. Due to their capability on capturing the size effects, and offering solutions independent of spatial discretization, enriched non-classical continuum theories are often more preferable with respect to the classical ones. In the present study, the sample problem of a plate with a circular inclusion subjected to a uniform tensile stress is investigated in terms of both 'implicit'/'weak' and 'explicit'/'strong' non-local descriptions: Cosserat (micropolar) and Eringen theories, by employing the finite element method. The material parameters of 'implicit' model is assumed to be known, while the nonlocality of 'explicit' model is optimized according to stress concentration factors reported for infinite Cosserat plates. The advantages/disadvantages, and correspondence/non-correspondence between both non-local models are highlighted and discussed apparently for the first time, by comparing the stress field provided for reference benchmark problem under various scale ratios, and material parameter combinations for matrix-inclusion pair. The results reveal the analogous character of both non-local models in case of geometric singularities, which may pave the way for further studies considering problems with noticeable scale effects and load singularities.

Keywords:

Non-local models; Cosserat; Eringen; nonhomogeneous solids; finite elements; scale effects

1 Introduction

When internal (e.g. atomic distance, size of heterogeneities, etc.) and external (e.g. wave length of loading conditions, sample length, etc.) time and/or length scales become comparable, the discrete nature of structure starts to play a key role on properly describing the overall mechanical behaviour. Since classical (local) theory of elasticity is incapable of capturing the size effects [**1-5**], and direct discrete modelling techniques are not practical due to their computational expense [**6-10**], enriched non-classical continuum theories [**11-16**] have been often proposed in the literature. Among them, the micropolar (Cosserat) theory [**17-19**] and Eringen's nonlocal theory [**16, 20, 21**], both of which incorporate size effects associated with the material's internal structure by different principles [**1-5**, **11-25**], will be the main object of this study.

Non-locality, by definition, implies the presence of internal lengths and spatial dispersion properties in wave propagation [**22**]. Within this framework, as suggested in [**13**, **14**, **23, 25**], we can distinguish between 'implicit'/'weak' and 'explicit'/'strong' non-local formulations. The former is referred to continua with extra degrees of freedom of various kind (i.e. [**12, 14, 15**]), in which there exist additional equations of motion containing non-standard primal fields, named generalised continua, microcontinua, or even multifield continua. While in the latter (i.e. [**16**, **20**, **21**]) primal fields of classical elasticity are preserved, yet the equations of motion contain integral, integro-differential or finite-difference operators in the spatial fields. In the end, both approaches avoid physical inadequacies, theoretical/computational problems related to ill-posedness in the field equations and mesh-dependency in numerical solutions [**1**,**2**].

Among 'implicit' non-local models, many papers showed the advantages of micropolar theory, which has been widely exploited for describing heterogeneous materials with microstructures (e.g. masonry-like structures, granular, blocked and layered materials, rock assemblages, reinforced composites, and so on [**26-33**]). The micropolar model was first developed by Cosserat brothers [**17**], and improved by many researchers over the years such as, Eringen [**18**]**,** Nowacki [**19**], etc. The theory accounts for the rotation of individual material points by integrating size effects through an additional kinematic and work-conjugated dynamic descriptors representing the material microstructure. Respectively, the stress tensor is expressed in terms of skew-symmetric stress and couple-stress parts. Due to its limited non-local character, the theory is classified as 'implicit' or 'weak' non-local model. Meanwhile, Eringen's nonlocal theory, which was first introduced by Kröner [**34**], Krumhansl [**35**], Kunin [**22**], and Eringen [**36**] and were further improved by Eringen and Edelen [**20**], and Eringen

[**16, 37, 38**], is extensively employed to investigate the mechanical behaviour of nano/micro sized structures (e.g. carbon nanotubes, graphene sheets, non-homogenous elastic continua, etc.) [**39-41**]. The theory possesses 'explicit' or 'strong' non-locality, since the small-scale parameter is integrated directly into the convolution type constitutive equation to capture the size effects. Accordingly, stress at each point is related to the strain of entire domain through an attenuation-type kernel function that contains information about internal length. As the internal lengths may have many different interpretations depending on the structure [**16**, **23**], 'explicit' non-local continua may also be used represent the material microstructure like 'implicit' one, even if it has often not.

As an inevitable outcome of widespread application of composite materials, the studies that have focused on quantifying the effect of heterogeneities through investigation of interface between inclusion and matrix materials gained speed. This problem has been widely studied considering both classical [**42**, **43**, **44**] and non-classical theories via employing different solution techniques. As examples of early studies focused on non-local models, Lubarda [**45**] provided the analytical solutions in the context of anti-plane strain couple-stress elasticity, while Zhang and Sharma [**46**] employed strain gradient elasticity with couple stresses. From a different point of view, Dong, Wang and Rubin [**47**], treated the interface as a finite thickness Cosserat shell/membrane medium and compared their results with explicit solutions. More recently, Atroshchenko et al. [**48**], modelled the matrix-inclusion structure as Cosserat media considering various material properties and showed the effect of imperfect and perfect interfaces via employing boundary element method (BEM), while Fantuzzi et al., [**32**] investigated the classical matrix-inclusion problem considering micropolar theory using both strong and standard forms of the finite element method.

Due to its rather complex character in the implementation, integral form of Eringen's non-local theory based finite element (FE) formulation, originally derived by Polizzotto [**49**], has been only conducted by a limited number of researchers. Pisano, Sofi and Fuschi [**50**] are the first ones, who implemented the FE formulation in a two-dimensional (2D) nonlocal elasticity context for solving boundary-value problems. Inherently, the inclusion problem was first addressed by the same authors on the basis of a so-called "enhanced" strain-difference based Eringen-type nonlocal model [**39**] via modelling a piecewise-homogenous domain [**51**, **52**]. Although the effect of the non-local material parameters on strain field was widely and clearly discussed, the studies are limited with square inclusion and the stress evaluation of mentioned problem is only recently examined by Pisano and Fuschi [**53**], who obtained spurious stress oscillations around the inclusion when full integration is considered.

After the descriptions of 'implicit' and 'explicit' non-locality had been suggested [**13**, **14**, **23**], Trovalusci [**25**] has focused on their definitions in a comparative way, for the first time. Yet, these different descriptions of non-locality have not been employed to study a common problem to look for possible correspondences and differences. With this motivation, in the present study, the effect of a circular inclusion as in particle and/or fibre reinforced composite materials is investigated on the basis of both Cosserat ('implicit') and the integral form of Eringen's two-phase local/nonlocal ('explicit') theories under uniaxial loading by employing the finite element method. Hence, Eringen's theory is not here used to model solids at atomistic scale, but rather the focus is on structures at a larger scale dominated by other kinds of discrete nature (e.g. heterogeneity) yielding an apparent non-local mechanical behaviour. The inclusion is incorporated into the model as a heterogeneity possessing different material properties than the surrounding matrix. The intrinsic length scale parameter of Cosserat model is assumed to be known while the non-locality of Eringen model is optimized using an evolutionary algorithm to minimize the difference between stress concentration factors obtained for infinite 'implicit' and 'explicit' non-local plates. After constitutive parameter detection of 'explicit' model, the plates are investigated under various material combinations for matrix-inclusion pair. To mimic the effect of both finite and infinite plates, wide range of edge lengths for a fixed radius of inclusion is considered. To the best of our knowledge, this represents the first attempt to investigate the possible analogous/dissimilar characters between conducted 'implicit' and 'explicit' non-local continuum theories in the simplified context of a two dimensional inclusion-matrix problem under plane strain assumption.

The paper is organized as follows. In Section 2, the governing equations are outlined, and corresponding finite element formulations are derived in the context of both 'implicit' and 'explicit' non-local theories. Section 3 is devoted to numerical examination of matrix-inclusion problem, alongside with a brief explanation about optimization process. The comparison of 'explicit' and 'implicit' type non-local theories and the influence of small-scale parameters are also discussed focusing on the normal stress field. Finally, some concluding remarks about capabilities, advantages/disadvantages of both non-local models are presented in Section 4.

2 Materials and methods

Continuum theories considered in the present study are briefly explained, and the displacement-based finite element formulations are derived regarding two-dimensional plane-strain problems within the linearized kinematical framework. Matrix and inclusion are assumed as linear, elastic and isotropic materials possessing different mechanical properties. FE formulation of

micropolar continuum model is implemented within the environment of the software COMSOL Multiphysics© [**54**], while for Eringen's nonlocal model an in-house code is developed using Wolfram Mathematica [**55**]. The superscripts *E* and *M*, that refer to Eringen's and micropolar model, respectively, are used to distinguish the parameters appearing in both theories, and possessing different interpretations.

The body under investigation can be regarded as a set of material points in 3D Euclidean space, occupying a domain Ω_0, and enclosed with a boundary, Γ_0 which is subjected to traction vector, $\bar{\mathbf{t}}$, and couple-traction vector, $\overline{\mathbf{m}}$ (considered for Cosserat media only). A Cartesian coordinate system *xyz* is used with a suitable origin for the parameterization of positions of material points, **x**. In the two-dimensional framework (2D) it is assumed that Ω_0 is formed with a uniform and symmetric thickening of a 2D region $\Omega \in \{x, y\}$, enclosed with boundary Γ, along *z* axis by an amount of *h*.

2.1 Micropolar model

2.1.1 Overview

In micropolar theory, material particles that constitute continuum are described in terms of both their positions and orientations leading to following linearized kinematic relations:

$$\varepsilon_{ij}^{M} = u_{i,j} + e_{ijk}\phi_k, \quad \chi_{kj} = \phi_{k,j} \tag{1}$$

where ϕ_k stands for the components of micro-rotation vector, and ε_{ij}^{M} and χ_{kj} denote the components of strain and curvature tensors with e_{ijk} being the usual third-order permutation tensor. One may recognize that, if the micro-rotations are constrained to follow the local rigid rotations, (macro-rotations):

$$\phi_i = -\frac{1}{2} e_{ijk} u_{j,k} \tag{2}$$

the classical kinematic relations, i.e., $\varepsilon_{ij} = \left(u_{i,j} + u_{j,i}\right)/2$, will be recovered and the continuum becomes a couple-stress continuum [**26**, **56**].

From balance considerations, each component of surface traction and surface couple-traction, denoted by t_i^M and m_k, respectively, are described as:

$$t_i^M = \sigma_{ij}^M n_j, \quad m_k = \mu_{kj} n_j \tag{3}$$

where σ_{ij}^{M} and μ_{kj} are the components of the non-symmetric stress and couple-stress tensors, respectively, and n_j being the components of unit outward normal vector of the continuum boundary. Hence, if body forces and body couples are neglected, the equilibrium equations take the following form

$$\sigma_{ij,j}^{M} = 0, \quad \mu_{kj,j} - e_{ijk}\sigma_{ij}^{M} = 0 \tag{4}$$

Considering linear elasticity, the stress-strain relation of an isotropic micropolar continua can be represented as:

$$\sigma_{ij}^{M} = \lambda\varepsilon_{kk}^{M}\delta_{ij} + (\mu + \chi)\varepsilon_{ij}^{M} + \mu\varepsilon_{ji}^{M}, \quad \mu_{kj} = \alpha\chi_{ii}\delta_{kj} + \beta\chi_{jk} + \gamma\chi_{kj} \tag{5}$$

which requires six elastic material constants for the complete description, i.e., Lamé's constants λ and μ, and four additional parameters, α, β, γ and χ related to micropolar theory [**57**]. It is important to note that, in the present work, second Lamé's parameter, μ, is not equal to shear modulus, G, as in the classical convention, but holds following relation:

$$G = \mu + \frac{\chi}{2} \tag{6}$$

Accordingly, Poisson's ratio, ν, can be described as follows:

$$\nu = \frac{\lambda}{2(\lambda + G)} = \frac{\lambda}{2\lambda + 2\mu + \chi} \tag{7}$$

In Cosserat model, the size effects and relative rotations are incorporated through an internal characteristic length, l_c, and a coupling number, N, in such a way that:

$$l_c^2 = \frac{\gamma}{2(2\mu + \chi)}, \quad N^2 = \frac{\chi}{2(\mu + \chi)} \tag{8}$$

If these parameters (i.e. l_c, N) are taken small enough. the Cosserat effects become negligible and the body behaves as Cauchy continua. Note that this finding is valid only in the case of materials with at least the orthotetragonal symmetry, or materials belonging to more restricted symmetry classes, as of course isotropic materials [**26**, **58**].

2.1.2 Finite Element Formulation

For FE modelling, the field variables within an element e (i.e. $\mathbf{u}_e$, $\boldsymbol{\varphi}_e$) are approximated considering a natural coordinate system ζ, η and using related interpolation function matrices:

$$\mathbf{u}_e = \mathbf{N}_u^{M}\,\widetilde{\mathbf{u}}_e, \quad \boldsymbol{\varphi}_e = \mathbf{N}_{\phi}\,\widetilde{\boldsymbol{\varphi}}_e \tag{9}$$

where the over tilde symbol is used to indicate the nodal values. Since the present study restrained with 2D media only, the degrees of freedom (DOFs) per each point is reduced to two

in-plane displacement components along *x* and *y* directions, i.e., u_x and u_y, and one out-of-plane micro-rotation component along *z* direction, i.e., ϕ_z.

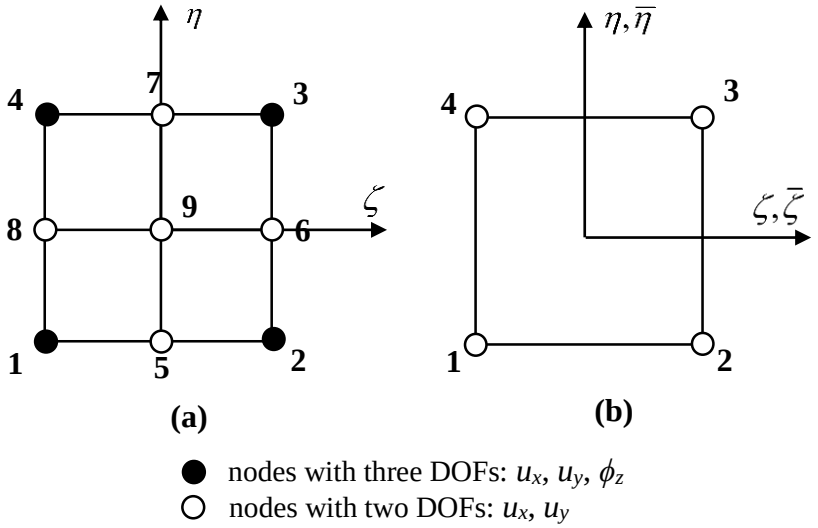

Fig. 1 The **(a)** 9-node quadrangular, **(b)** 4-node quadrilateral element illustrated in natural coordinate system ($-1 \le \eta \le 1, -1 \le \zeta \le 1$).

$\mathbf{N}_u^M$ is employed for interpolation of nodal in-plane displacements and consists of quadratic interpolation functions, while $\mathbf{N}_\phi$ is employed for nodal out-of-plane micro-rotations, and includes linear type shape functions. As it was mentioned in Fantuzzi et al., [**32**], and Fantuzzi et al., [**33**], and clearly showed in the **Fig. 1(a)**, all the nodes of the nine-node Lagrange element possess displacement-type DOFs, whereas micro-rotation DOFs are attached only to the four corner nodes:

$$\mathbf{N}_u^M = \begin{bmatrix} N_u^1 & 0 & \cdots & N_u^9 & 0 \\ 0 & N_u^1 & & 0 & N_u^9 \end{bmatrix}, \quad \mathbf{N}_\phi = \begin{bmatrix} N_\phi^1 & \cdots & N_\phi^4 \end{bmatrix} \tag{10}$$

Accordingly, strain and curvature fields, that are ordered in vectors;

$$\boldsymbol{\varepsilon}_e^M = \begin{bmatrix} \varepsilon_{xx}^M & \varepsilon_{yy}^M & \varepsilon_{xy}^M & \varepsilon_{yx}^M \end{bmatrix}_e^{\mathrm{T}}, \qquad \boldsymbol{\chi}_e = \begin{bmatrix} \chi_{zx} & \chi_{zy} \end{bmatrix}_e^{\mathrm{T}} \tag{11}$$

are obtained using differential matrix operator, $\mathbf{L}^M$, permutation vector **M**, and gradient operator, ∇:

$$\boldsymbol{\varepsilon}_e^M = \mathbf{L}^M \mathbf{u}_e + \mathbf{M}\boldsymbol{\varphi}_e = \mathbf{L}^M \mathbf{N}_u^M \tilde{\mathbf{u}}_e + \mathbf{M}\mathbf{N}_\phi \tilde{\boldsymbol{\varphi}}_e = \begin{bmatrix} \mathbf{L}^M \mathbf{N}_u^M & \mathbf{M}\mathbf{N}_\phi \end{bmatrix} \begin{Bmatrix} \tilde{\mathbf{u}}_e \\ \tilde{\boldsymbol{\varphi}}_e \end{Bmatrix} = \mathbf{B}_{e\varepsilon}^M \mathbf{d}_e^M,$$

$$\boldsymbol{\chi}_e = \nabla \boldsymbol{\varphi}_e = \nabla\left(\mathbf{N}_\phi \tilde{\boldsymbol{\varphi}}_e\right) = \begin{bmatrix} 0 & \nabla \mathbf{N}_\phi \end{bmatrix} \begin{Bmatrix} \tilde{\mathbf{u}}_e \\ \tilde{\boldsymbol{\varphi}}_e \end{Bmatrix} = \mathbf{B}_{e\chi}^M \mathbf{d}_e^M \tag{12}$$

$$\mathbf{d}_e^M = \begin{Bmatrix} \tilde{u}_x^1 & \tilde{u}_y^1 & \cdots & \tilde{u}_x^9 & \tilde{u}_y^9 & \tilde{\phi}_z^1 & \cdots & \tilde{\phi}_z^4 \end{Bmatrix}_e^{\mathrm{T}}$$

where $\mathbf{d}_e^M$ indicates the unknown vector of nodal displacements, and the superscripts appeared in Eq. 12_3 (and also in Eq. 10) refer to node numbers, while the matrices $\mathbf{B}_{e\varepsilon}^M$ and $\mathbf{B}_{e\chi}^M$ include the derivation of interpolation functions considering following relations

$$\mathbf{L}^M = \begin{bmatrix} \dfrac{\partial}{\partial x} & 0 & \dfrac{\partial}{\partial y} & 0 \\ 0 & \dfrac{\partial}{\partial y} & 0 & \dfrac{\partial}{\partial x} \end{bmatrix}^{\mathrm{T}}, \quad \mathbf{M} = \begin{bmatrix} 0 & 0 & 1 & -1 \end{bmatrix}^{\mathrm{T}}, \quad \nabla = \begin{bmatrix} \dfrac{\partial}{\partial x} & \dfrac{\partial}{\partial y} \end{bmatrix}^{\mathrm{T}} \tag{13}$$

Since $\mathbf{N}_u^M$ and $\mathbf{N}_\phi$ are taken as functions of natural coordinates, the derivations with respect to physical coordinate systems given in Eq. 13_1 and Eq. 13_2 should be performed using chain rule, and inverse Jacobian matrix of element *e*, $\mathbf{J}_e^{-1}$. Inherently, constitutive relations given in Eq. 5 are transformed to:

$$\boldsymbol{\sigma}_e^M = \mathbf{D}_{e\varepsilon}^M \mathbf{B}_{e\varepsilon}^M \mathbf{d}_e^M, \quad \boldsymbol{\mu}_e = \mathbf{D}_{e\chi}^M \mathbf{B}_{e\chi}^M \mathbf{d}_e^M \tag{14}$$

where $\boldsymbol{\sigma}_e^M$ and $\boldsymbol{\mu}_e$ vectors, described as

$$\boldsymbol{\sigma}_e^M = \begin{bmatrix} \sigma_{xx}^M & \sigma_{yy}^M & \sigma_{xy}^M & \sigma_{yx}^M \end{bmatrix}_e^{\mathrm{T}}, \quad \boldsymbol{\mu}_e = \begin{bmatrix} \mu_{zx} & \mu_{zy} \end{bmatrix}_e^{\mathrm{T}} \tag{15}$$

denote non-symmetric stress field and couple stress field of an element, while constitutive matrices, $\mathbf{D}_{e\varepsilon}^M$ and $\mathbf{D}_{e\chi}^M$ are defined as follows:

$$\mathbf{D}_{e\varepsilon}^M = \begin{bmatrix} \lambda + 2G & \lambda & 0 & 0 \\ \lambda & \lambda + 2G & 0 & 0 \\ 0 & 0 & G + \chi/2 & G - \chi/2 \\ 0 & 0 & G - \chi/2 & G + \chi/2 \end{bmatrix}, \quad \mathbf{D}_{e\chi}^M = \begin{bmatrix} \gamma & 0 \\ 0 & \gamma \end{bmatrix} \tag{16}$$

A standard displacement-based FE formulation is provided using the principle of minimum total potential energy, where for the static analysis, total potential energy functional, Π^M, which is written in terms of total elastic strain energy, U^M and external work potential W^M:

$$\begin{aligned} \Pi^M &= U^M + W^M \\ U^M &= \frac{h}{2} \sum_{m=1}^{N_{total}} \iint_{A_m} \left(\left(\boldsymbol{\varepsilon}_m^M \right)^{\mathrm{T}} \boldsymbol{\sigma}_m^M + \left(\boldsymbol{\chi}_m \right)^{\mathrm{T}} \boldsymbol{\mu}_m \right) \mathrm{d}A_m \\ W^M &= -\sum_{m=1}^{N_{total}} \iint_{\Gamma_m} \left(\mathbf{d}_m^M \right)^{\mathrm{T}} \begin{Bmatrix} \left(\mathbf{N}_u^M \right)^{\mathrm{T}} \bar{\mathbf{t}} \\ \left(\mathbf{N}_\phi \right)^{\mathrm{T}} \overline{\mathbf{m}} \end{Bmatrix} \mathrm{d}\Gamma_m \quad \left(\text{in the absence of body forces and couples} \right) \end{aligned} \tag{17}$$

must be minimum for equilibrium:

$$\frac{\partial \Pi^M \left[\mathbf{d}^M \right]}{\partial \mathbf{d}_i^M} = 0, \left(i = 1, 2, \ldots, N_{total} \right) \tag{18}$$

with N_{total}, A_m and $\mathbf{d}^M$ being the total number of elements, area of mth element, and global nodal displacement vector. One can see that, Eq. 18 is simplified to following form,

$$\frac{\partial \Pi^M\left[\mathbf{d}_1^M\right]}{\partial \mathbf{d}_1^M}=\frac{\partial \Pi^M\left[\mathbf{d}_2^M\right]}{\partial \mathbf{d}_2^M}=\ldots=\frac{\partial \Pi^M\left[\mathbf{d}_{N_{total}}^M\right]}{\partial \mathbf{d}_{N_{total}}^M}=0 \tag{19}$$

since the remaining terms (e.g. $\partial \Pi^M\left[\mathbf{d}_1^M\right]/\partial \mathbf{d}_2^M$, $\partial \Pi^M\left[\mathbf{d}_1^M\right]/\partial \mathbf{d}_3^M$,…) vanish due to 'weak' non-local character of constitutive equation. Accordingly, the stiffness matrix of an element m is derived as:

$$\frac{\partial U^M}{\partial \mathbf{d}_m^M}=\underbrace{\left(\underbrace{h\int_{-1}^{1}\int_{-1}^{1}\left(\mathbf{B}_{m\varepsilon}^M\right)^{\mathrm{T}}\mathbf{D}_{m\varepsilon}^M\,\mathbf{B}_{m\varepsilon}^M\,\det\left|\mathbf{J}_m\right|\mathrm{d}\zeta\,\mathrm{d}\eta}_{\mathbf{k}_{m\varepsilon}^M}+\underbrace{h\int_{-1}^{1}\int_{-1}^{1}\left(\mathbf{B}_{m\chi}^M\right)^{\mathrm{T}}\mathbf{D}_{m\chi}^M\,\mathbf{B}_{m\chi}^M\,\det\left|\mathbf{J}_m\right|\mathrm{d}\zeta\,\mathrm{d}\eta}_{\mathbf{k}_{m\chi}^M}\right)}_{\mathbf{k}_m^M}\mathbf{d}_m^M \tag{20}$$

By including the derivative of external work potential, and performing the proper assemblage operations, the well-known linear equation system is achieved:

$$\mathbf{K}^M\,\mathbf{d}^M=\mathbf{f}^M \tag{21}$$

where $\mathbf{K}^M$, and $\mathbf{f}^M$ refer to global stiffness matrix, and global nodal force vector of discretized 2D micropolar media. For integration operations in Eqs. 17 and 20, a standard Gauss integration technique is adopted.

2.2 Eringen's two-phase local/nonlocal model

2.2.1 Overview

The assumptions of linear elasticity provide the following kinematic relations for Eringen's nonlocal model:

$$\varepsilon_{ij}^E=\frac{1}{2}\left(u_{i,j}+u_{j,i}\right) \tag{22}$$

where ε_{ij}^E refer to components of the strain tensor. For the continuum to be in balance, interactions between material points, that are characterized through traction forces only, $\mathbf{t}^E$, can be described as follows:

$$t_i^E=\sigma_{ij}^E n_j \tag{23}$$

where σ_{ij}^E refers to components of the symmetric stress tensor. In the absence of body forces, the following equilibrium equation is carried out, similar to classical (local) elasticity theory:

$$\sigma_{ij,j}^E=0 \tag{24}$$

In fact, the localisation of global (integral) balance laws (e.g. mass, momentum, moment of momentum, energy) would introduce *non-local residuals* (*localisation residuals*) as declared by Eringen and Edelen [**20**] and Eringen [**21**, **37**]. This phenomenon appears due to the long-range effects of all material points of the body at a reference point, and would contradict with the state that the global balance laws are valid for each infinitesimal volume element isolated from the body [**16**, **20**, **21**, **37**]. However, with proposing a new interpretation for stress tensor and internal energy density, the local form of balance laws is recovered except for jump conditions [**16**]. Since for chemically inert bodies the contribution of non-local mass residual dies out, and as a result of axiom of objectivity the contribution of non-local body force residuals as well as non-local body couple residual should vanish, the only remaining residual associated with non-locality is the non-local energy residual. Nevertheless, as studied via Polizotto et al. [**39**] and Marotti de Sciarra [**59**], it is represented as a function of strain rate, hence omitted in the present study under the quasi-static condition and yielding following constitutive equation for linear elastic isotropic solids:

$$\sigma_{ij}^{E} = \xi\left(\lambda\varepsilon_{kk}^{E}\delta_{ij} + 2G\varepsilon_{ij}\right) + \left(1-\xi\right)\int_{\Omega_0}\tau\left(\left|\bar{\mathbf{x}}-\mathbf{x}\right|,\kappa\right)\left(\lambda\varepsilon_{kk}^{E}\left(\bar{\mathbf{x}}\right)\delta_{ij} + 2G\varepsilon_{ij}^{E}\left(\bar{\mathbf{x}}\right)\right)\mathrm{d}\Omega_0\left(\bar{\mathbf{x}}\right) \tag{25}$$

as also demonstrated in Eringen [**16**, **37**]. To avoid any conflict with its previous interpretation in micropolar model, constitutive equation is expressed using shear modulus, G, instead of second Lamé's parameter, μ, while first Lamé's parameter, λ, is retained. The convolution type constitutive equation of the integral form of Eringen's two phase local/nonlocal model implies that the stress at a point is linked to the strain of the entire domain through a kernel function, τ, which is assumed to be bi-exponential in the present study, in accordance with literature [**60**, **61**], and represented as follows:

$$\tau\left(r,\kappa\right) = \frac{\mathrm{e}^{-\frac{r}{\kappa}}}{2\pi^{d-1}\kappa^{d}} \tag{26}$$

where r (i.e. $r = \left|\mathbf{x}-\bar{\mathbf{x}}\right|$) refers to the Euclidian distance between investigated point of interest, $\mathbf{x}$, and its neighbour points, $\bar{\mathbf{x}}$, [**49, 51, 52**], and d being the dimension of the structure, while κ stands for nonlocal parameter. In fact, different type of kernel functions (e.g. bell-shaped, gauss-like, etc.), that could be more suitable for the problem under investigation exist, yet their influence will be reported in another forthcoming study of the authors. As one can see, two additional parameters, ξ and κ, both of which attribute to non-local character of structure, are introduced with Eringen's non-local theory. The former symbol stands for fraction coefficient, that ranges from 0 to 1, and is used to regulate the weights of local and non-local parts, while

the non-local parameter that depends on both internal length scale, a_0, and material constants e_0:

$$\kappa = e_0 a_0 \tag{27}$$

defines the characteristic of the kernel function. Hence, assuming ξ equals to 1 yields full local model, and 0 corresponds to full non-local one, while the increasing values of κ produces more pronounced non-locality.

2.2.2 Finite Element Formulation

For FE modelling of 2D non-local media, the domain is discretized using four-node quadrilateral elements (see **Fig. 1 (b)**), and displacement field within an element e (i.e. $\mathbf{u}_e$) is approximated using interpolation matrix including linear shape functions, $\mathbf{N}_u$, and nodal displacement vector, $\mathbf{d}_e^E$ as in the form:

$$\begin{aligned}
&\mathbf{u}_e = \mathbf{N}_u^E \mathbf{d}_e^E \\
&\mathbf{N}_u^E = \begin{bmatrix} N_u^1 & 0 & \cdots & N_u^4 & 0 \\ 0 & N_u^1 & & 0 & N_u^4 \end{bmatrix} \\
&\mathbf{d}_e^E = \begin{Bmatrix} \widetilde{u}_x^1 & \widetilde{u}_y^1 & \widetilde{u}_x^2 & \widetilde{u}_y^2 & \widetilde{u}_x^3 & \widetilde{u}_y^3 & \widetilde{u}_x^4 & \widetilde{u}_y^4 \end{Bmatrix}_e^{\mathrm{T}}
\end{aligned} \tag{28}$$

Corresponding approximate strain field within an element e, i.e., $\boldsymbol{\varepsilon}_e^E = \begin{bmatrix} \varepsilon_{xx}^E & \varepsilon_{yy}^E & 2\varepsilon_{xy}^E \end{bmatrix}_e^T$, is then defined as:

$$\begin{aligned}
&\boldsymbol{\varepsilon}_e^E = \mathbf{L}^E \mathbf{N}_u^E \mathbf{d}_e^E = \mathbf{B}_e^E \mathbf{d}_e^E \\
&\mathbf{L}^E = \begin{bmatrix} \dfrac{\partial}{\partial x} & 0 & \dfrac{\partial}{\partial y} \\ 0 & \dfrac{\partial}{\partial y} & \dfrac{\partial}{\partial x} \end{bmatrix}^T
\end{aligned} \tag{29}$$

where $\mathbf{L}^E$ and $\mathbf{B}_e^E$ refer to differential operator, and strain matrices. As previously mentioned, the derivations with respect to physical coordinate systems given in Eq. 29_2 are performed by the chain rule, and employing the inverse of Jacobian matrix of element e, $\mathbf{J}_e^{-1}$. The constitutive relation given in Eq. 25 is then transformed to:

$$\boldsymbol{\sigma}_e^E = \xi_e \mathbf{D}_e^E \mathbf{B}_e^E \mathbf{d}_e^E + (1-\xi_e) \sum_{i=1}^{N_{totgl}} \int_{-1}^{1} \int_{-1}^{1} \frac{\mathrm{e}^{-\frac{r}{\kappa}}}{2\pi\kappa^2} \mathbf{D}_i^E \overline{\mathbf{B}}_i^E \mathbf{d}_i^E \det\left|\overline{\mathbf{J}}_i\right| \mathrm{d}\overline{\zeta}\, \mathrm{d}\overline{\eta} \tag{30}$$

while stress tensor and constitutive matrix are described as below:

$$\boldsymbol{\sigma}_e^E = \begin{bmatrix} \sigma_{xx}^E & \sigma_{yy}^E & \sigma_{xy}^E \end{bmatrix}_e^T, \quad \mathbf{D}_e^E = \begin{bmatrix} \lambda+2G & \lambda & 0 \\ \lambda & \lambda+2G & 0 \\ 0 & 0 & G \end{bmatrix}_e \tag{31}$$

Note that the over bar in Eq. 30, denotes that the related matrix is written in terms of $\bar{\zeta}, \bar{\eta}$ as a requirement of convolution form of Eringen's constitutive relation, hence, should not be confused with overbars in prescribed surface traction, $\bar{\mathbf{t}}$, and surface couple-traction, $\overline{\mathbf{m}}$.

Finally, the weak form of displacement based FE formulation is derived based on minimum total potential energy principle as explained previously,

$$\Pi^E = U^E + W^E$$

$$U^E = \frac{h}{2}\sum_{m=1}^{N_{total}} \iint_{A_m} \left(\boldsymbol{\varepsilon}_m^E\right)^{\mathrm{T}} \boldsymbol{\sigma}_m^E \, \mathrm{d}A_m \tag{32a}$$

$$W^E = -\sum_{m=1}^{N_{total}} \iint_{\Gamma_m} \left(\mathbf{d}_m^E\right)^{\mathrm{T}} \left(\mathbf{N}_u^E\right)^{\mathrm{T}} \bar{\mathbf{t}} \, \mathrm{d}\Gamma_m \quad \left(\text{in the absence of body forces}\right)$$

$$\frac{\partial \Pi^E\left[\mathbf{d}^E\right]}{\partial \mathbf{d}_i^E} = 0, \ (i = 1, 2, \ldots, N_{total}) \tag{32b}$$

However as different from micropolar model, in Eringen's nonlocal theory, all derivatives (e.g. $\partial\Pi^E\left[\mathbf{d}_1^E\right]/\partial\mathbf{d}_2^E, \partial\Pi^E\left[\mathbf{d}_1^E\right]/\partial\mathbf{d}_3^E, \ldots$) are recovered due to its 'strong' non-local character, and resulting stiffness matrix is attained for an element *m*:

$$\begin{aligned}
\frac{\partial U_{FEM}^M}{\partial \mathbf{d}_m^E} = {} & \xi_m \underbrace{h\int_{-1}^{1}\int_{-1}^{1} \left(\mathbf{B}_m^E\right)^T \mathbf{D}_m^E \mathbf{B}_m^E \det\left|\mathbf{J}_m\right| \mathrm{d}\zeta \, \mathrm{d}\eta}_{\mathbf{k}_m^E} \mathbf{d}_m^E \\
& + \left(1-\xi_m\right) \underbrace{h\int_{-1}^{1}\int_{-1}^{1}\int_{-1}^{1}\int_{-1}^{1} \frac{\mathrm{e}^{-\frac{r}{\kappa}}}{2\pi\kappa^2} \left(\mathbf{B}_m^E\right)^T \mathbf{D}_m^E \overline{\mathbf{B}}_m^E \det\left|\overline{\mathbf{J}}_m\right| \det\left|\mathbf{J}_m\right| \mathrm{d}\bar{\zeta} \, \mathrm{d}\bar{\eta} \mathrm{d}\zeta \, \mathrm{d}\eta}_{\mathbf{k}_{mm}^E} \mathbf{d}_m^E \\
& + \left(1-\xi_m\right) \sum_{\substack{n \\ n\neq m}} \underbrace{\frac{h}{2}\int_{-1}^{1}\int_{-1}^{1}\int_{-1}^{1}\int_{-1}^{1} \frac{\mathrm{e}^{-\frac{r}{\kappa}}}{2\pi\kappa^2} \left(\mathbf{B}_m^E\right)^T \mathbf{D}_n^E \overline{\mathbf{B}}_n^E \det\left|\overline{\mathbf{J}}_n\right| \det\left|\mathbf{J}_m\right| \mathrm{d}\bar{\zeta} \, \mathrm{d}\bar{\eta} \mathrm{d}\zeta \, \mathrm{d}\eta}_{\mathbf{k}_{mn}^E} \mathbf{d}_n^E \\
& + \left(1-\xi_n\right) \sum_{\substack{n \\ n\neq m}} \underbrace{\left(\frac{h}{2}\int_{-1}^{1}\int_{-1}^{1}\int_{-1}^{1}\int_{-1}^{1} \frac{\mathrm{e}^{-\frac{r}{\kappa}}}{2\pi\kappa^2} \left(\mathbf{B}_n^E\right)^T \mathbf{D}_m^E \overline{\mathbf{B}}_m^E \det\left|\overline{\mathbf{J}}_m\right| \det\left|\mathbf{J}_n\right| \mathrm{d}\bar{\zeta} \, \mathrm{d}\bar{\eta} \mathrm{d}\zeta \, \mathrm{d}\eta \right)^T}_{\left(\mathbf{k}_{nm}^E\right)^T} \mathbf{d}_n^E
\end{aligned} \tag{33}$$

The subscripts *m* and *n* stand for element number. The term with coefficient ξ represents the local part of two-phase model, while the terms with coefficient $1-\xi$ correspond to the non-

local part. In the non-local part, the first term stands for the contribution of the *m*th element to its own energy, while second and third terms account for the influence exerted on the *m*th element by the remaining elements, and the influence exerted by the *m*th element to other elements, respectively. Second and third terms in the non-local part, which expand element stiffness matrix to overall dimension are equal to each other only for homogenous material properties:

$$\mathbf{k}_{mn}^{E} = \left(\mathbf{k}_{nm}^{E}\right)^{T} \quad \text{for} \quad \mathbf{D}_{n}^{E} = \mathbf{D}_{m}^{E} \tag{34}$$

Finally, by including the derivative of external work potential, $\mathbf{f}_{m}^{E}$ the formulation of the *m*th element is provided:

$$\mathbf{f}_{m}^{E} = \xi_m \mathbf{k}_{m}^{E} \mathbf{d}_{m}^{E} + \left(1-\xi_m\right)\mathbf{k}_{mm}^{E}\mathbf{d}_{m}^{E} + \left(1-\xi_m\right)\sum_{n=1,\, n\neq m}^{N_{total}} \mathbf{k}_{mn}^{E}\mathbf{d}_{n}^{E} + \left(1-\xi_n\right)\sum_{n=1,\, n\neq m}^{N_{total}} \left(\mathbf{k}_{nm}^{E}\right)^{T}\mathbf{d}_{n}^{E} \tag{35}$$

One can see that, Eqs. 33 and 35 have the same nature with the corresponding ones reported in literature [**47**], and to be accordance with the literature, $\mathbf{k}_{mn}^{E}$ and $\mathbf{k}_{nm}^{E}$ are called as cross-stiffness matrices from now on. At last, the following linear equation system is obtained after proper assemblage operations.

$$\mathbf{K}^{E}\,\mathbf{d}^{E} = \mathbf{f}^{E} \tag{36}$$

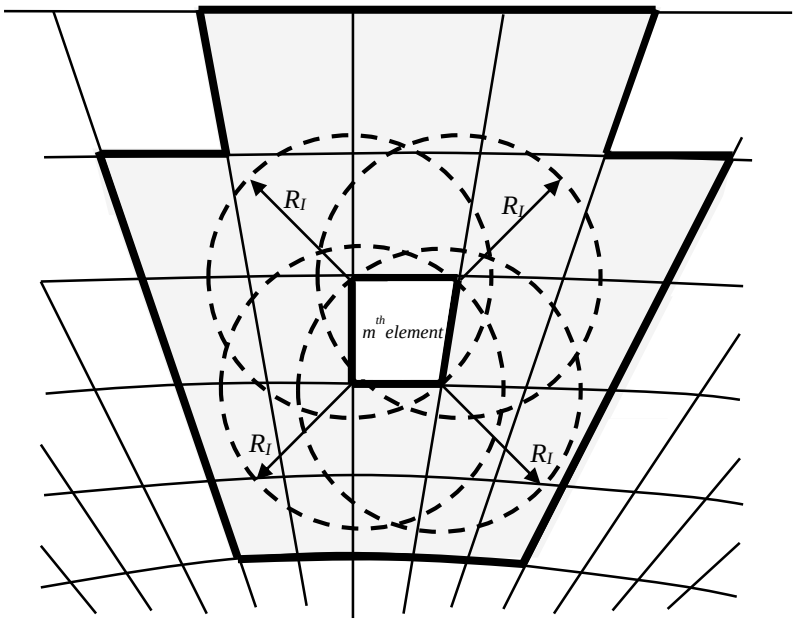

Fig. 2 Illustration of the influence zone of a quadrilateral element *m* (Neighbour elements that fall within the zone, and contribute to the stiffness matrix of element *m* are shown in grey)

The integration operations given in Eq. 33 are performed using GQ method. For the local part (i.e. $\mathbf{k}_m$), 2 x 2 Gauss sampling points are sufficient, while for the nonlocal part, the number of Gauss sampling points varies depending on nonlocal parameter, element length and calculated part of stiffness matrix (i.e. $\mathbf{k}_{mm}$ or $\mathbf{k}_{mn}$). To reduce the computational burden, only the elements inside the influence zone (see **Fig. 2**) are assumed to contribute to cross-stiffness matrices $\mathbf{k}_{mn}$ and $\mathbf{k}_{nm}$, while the effect of others is negligible due to the decaying nature of attenuation function [**50, 62**]. It should also be noted that, this simplification inherently leads to some sort of banding of the global stiffness matrix $\mathbf{K}^E$.

3 Numerical Simulations

This section is devoted to the numerical examination of linear elastic plates with a circular inclusion under uniform tensile stress. As loading condition, a constant tensile stress of 100 [MPa] is applied to left and right vertical boundary edges, while boundary conditions are imposed by limiting the horizontal and vertical displacements of vertical and horizontal axes located in the middle, respectively (**Fig. 3**).

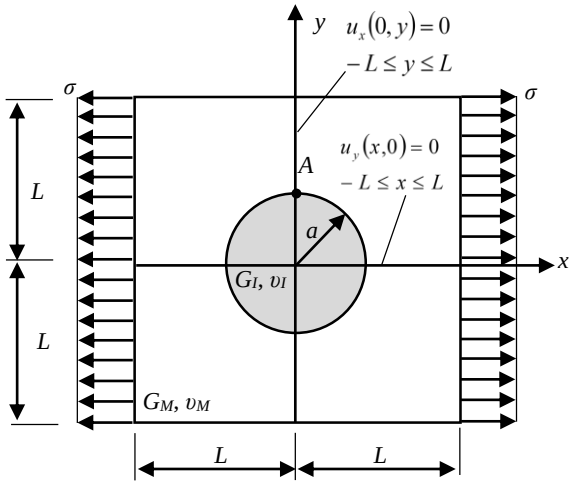

Fig. 3 Geometry, boundary and loading conditions of a square plate containing a circular inclusion.

Despite the symmetric character of the problem (along both *x* and *y* axes), analyses are performed regarding the full domain, since in the context of Eringen's nonlocal theory, imposing symmetry is much more complicated than only considering the symmetric part of the model [**63**]. It is a result of the missing neighbour elements that should have contributed to cross-stiffness matrices due to long-range interactions. The simulations are repeated considering two different mesh configurations of different refinement, both characterized by different scale ratios: for all models, respectively named Model 1, 2, 3, the radius of inclusion,

a, is assumed constant, 0.05 [m], while the width of the plate (structural/macro length), *L*, is modified in size: *L*/*a* = 3.0, 10.0, 20.0 to consider both finite and infinite domains (see **Fig. 4**).

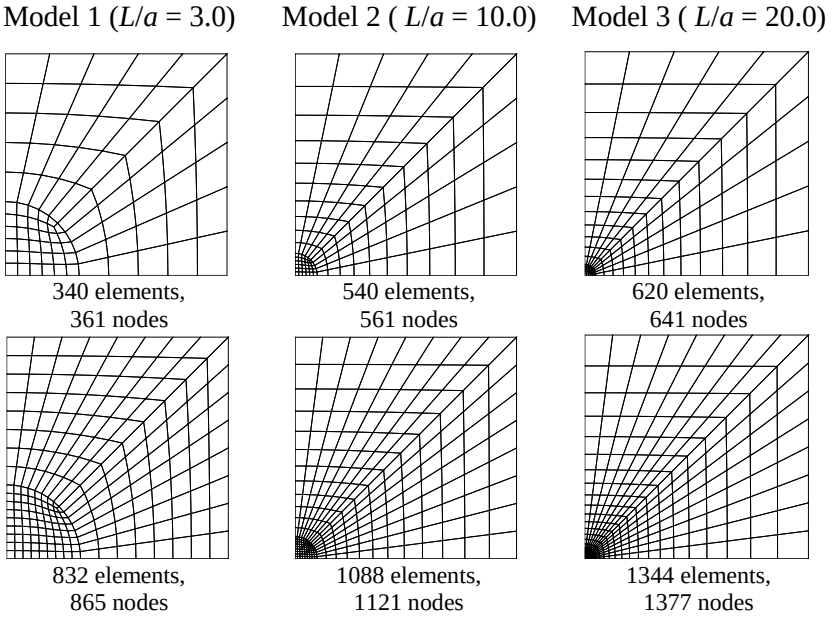

Fig. 4 Mesh configuration (top: coarse mesh, bottom: fine mesh) of the three Models

As the main purpose of the present study, the effect of different material configurations (see **Table 1**) is studied in the context of two distinct non-classical theories, Cosserat (micropolar) and Eringen' nonlocal models, as described below:

Mat (1): Both the matrix and the inclusion are modelled as Cauchy.

Mat (2): The inclusion is Cauchy and the matrix is Cosserat/Eringen.

Mat (3): The inclusion is Cosserat/Eringen and the matrix is Cauchy.

Mat (4): Both the matrix and inclusion are modelled as Cosserat/Eringen.

Table 1 Dimensionless material data for matrix-inclusion pairs.

	Eringen's Nonlocal T.		Cosserat (Micropolar) T.	
	Inclusion	Matrix	Inclusion	Matrix
Mat (1)	$\xi = 1.0$	$\xi = 1.0$	$l_c / a = 0.001$ $N = 0.001$	$l_c / a = 0.001$ $N = 0.001$
Mat (2)	$\xi = 1.0$	$\kappa / a = 0.2$ $\xi = \xi_{opt}$	$l_c / a = 0.001$ $N = 0.001$	$l_c / a = 1.0$ $N = 0.9$
Mat (3)	$\kappa / a = 0.2$ $\xi = \xi_{opt}$	$\xi = 1.0$	$l_c / a = 1.0$ $N = 0.9$	$l_c / a = 0.001$ $N = 0.001$
Mat (4)	$\kappa / a = 0.2$ $\xi = \xi_{opt}$	$\kappa / a = 0.2$ $\xi = \xi_{opt}$	$l_c / a = 1.0$ $N = 0.9$	$l_c / a = 1.0$ $N = 0.9$

In this way, it is aimed to examine the incorporation of size effects through 'implicit' and 'explicit' non-local, scale dependent continua, specifically focusing on stress concentration factor (SCF) as one of the main design parameters for the problem under investigation:

$$\mathrm{SCF} = \frac{\sigma_{\max}}{\sigma_0} \tag{37}$$

where σ_0 and $\sigma_{\max}$ correspond to nominal stress and maximum stress (e.g. obtained at interface point A), respectively.

For the transition between Cauchy (classical) and Cosserat/Eringen (non-classical) models, different strategies are developed based on the conducted continuum theory. For micropolar theory, it is achieved via tailoring the value of internal characteristic length, l_c and coupling number, N, as given in **Table 1**. For small values of corresponding material parameters, the size effect becomes negligible, and the model behaves as a Cauchy continuum, while an opposite trend is obtained for larger values. On the other hand, when Eringen's nonlocal theory is considered, the locality and/or non-locality of inclusion and matrix can simply be arranged by changing the fraction coefficient, ξ, and/or the non-local parameter, κ, appearing in the constitutive equation. For a fully local media, fraction coefficient should be equal to unity (i.e. ξ =1), while any smaller value (i.e. ξ <1) lets the incorporation of size effects. To modify the non-locality of Eringen's model in accordance with micropolar theory (regarding the sample problem), an evolutionary algorithm called Differential Evolution Method [**64**], which has been widely employed as a global optimization tool in engineering problems, is utilized. To this aim, it is intended to reduce the relative difference between stress concentration factors obtained through Eringen's nonlocal theory based FE models (for L/a = 20.0) and explicit expressions of stress concentration factors reported for infinite plates employing Cosserat theory [**48**]. As it is less expensive computationally, the parameter to be optimized is selected as ξ ($0.0 \le \xi \le 1.0$), while κ is taken as $0.2a$ [m] for all the models, and the radius of influence zone (i.e. R_I), is assumed as 0.05 [m] for given κ. It should be noted that, although an arbitrary value in accordance with literature [**53**] is assigned for κ, the attention was paid to keep it reasonable in comparison with radius of inclusion. Eventually, the objective function to be minimized, takes the following form.

$$\mathrm{OF} = \left\|\mathbf{f}(\xi)\right\|, \qquad \mathbf{f}(\xi) = \left\{ \left| \frac{\mathrm{SCF_E}(\xi)}{\mathrm{SCF_C}} - 1 \right|_{(2)}, \quad \left| \frac{\mathrm{SCF_E}(\xi)}{\mathrm{SCF_C}} - 1 \right|_{(3)}, \quad \left| \frac{\mathrm{SCF_E}(\xi)}{\mathrm{SCF_C}} - 1 \right|_{(4)} \right\}^{\mathrm{T}} \tag{38}$$

where the double bracket refers to norm operation, the subscripts E and C stand for Eringen

and Cosserat models, respectively, and the sub-numbers in parenthesis correspond to the material configurations (i.e. Mat (2), Mat (3), Mat (4)). The numerical values of parameters used for different material configurations can be found in **Table 2**.

Table 2 Material properties of matrix and inclusion pairs

		Inclusion				Matrix			
		1	2	3	4	1	2	3	4
Eringen Nonlocal Theory	G (GPa)	0.5	0.5	0.5	0.5	1.0	1.0	1.0	1.0
	ν	1/4	1/4	1/4	1/4	1/3	1/3	1/3	1/3
	κ (m)	-	-	0.01	0.01	-	0.01	-	0.01
	ξ	1.0	1.0	ξ_{opt}	ξ_{opt}	1.0	ξ_{opt}	1.0	ξ_{opt}
Micropolar Theory	G (GPa)	0.5	0.5	0.5	0.5	1.0	1.0	1.0	1.0
	μ (GPa)	0.4999	0.4999	-1.632	-1.632	0.999	-3.263	0.999	-3.263
	ν	1/4	1/4	1/4	1/4	1/3	1/3	1/3	1/3
	l_c (m)	5.10^{-5}	5.10^{-5}	0.05	0.05	5.10^{-5}	0.05	5.10^{-5}	0.05
	N	0.001	0.001	0.9	0.9	0.001	0.9	0.001	0.9
	χ (GPa)	1.10^{-6}	1.10^{-6}	4.2632	4.2632	2.10^{-6}	8.5263	2.10^{-6}	8.5263
	γ (kN)	0.005	0.005	5.10^{3}	5.10^{3}	0.01	1.10^{5}	0.01	1.10^{5}

Before any further progress, the procedure that is followed to attain nodal stresses should be explained. After the normal stress field of an element that is obtained in terms of natural coordinates is directly used to calculate the stresses at nodes of corresponding element (i.e. *direct evaluation* method), single nodal stress values are calculated by averaging the stress contribution of all the elements sharing the corresponding node. Note that, this approach is valid only if the nodes are surrounded by the elements possessing same kind of material properties. Hence, to obtain the correct stress values for interfacial nodes (e.g. point A), the contributions of matrix and inclusion elements are handled separately resulting in two distinct values.

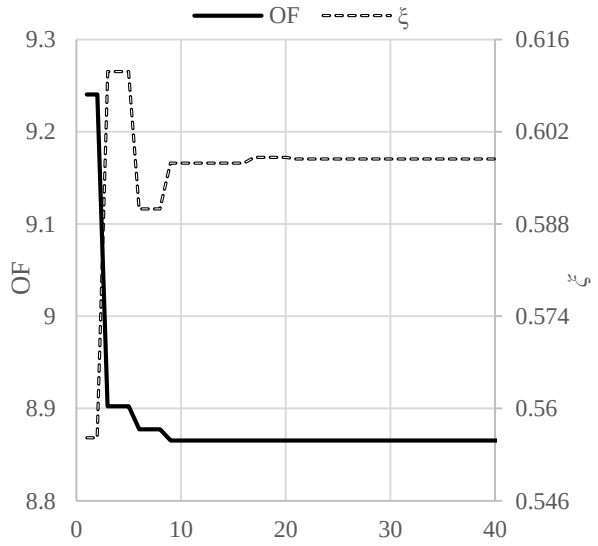

Fig. 5 Rate of convergence during optimization of fraction coefficient (*x* axis refers to iteration number)

It is assumed that, the optimization is achieved either the total number of stall iterations exceeds 50, or the objective function is minimized up to 0.1%. For this problem, the former condition is fulfilled and optimum fraction coefficient is obtained as: $\xi_{opt} = 0.597873$ with a convergence rate illustrated in **Fig. 5.** Once the nonlocal material parameters of Eringen's model are fixed, the results of finite element plate models employing either Eringen or Cosserat theories are analysed considering all scale ratios, material configurations, and domain discretization. Corresponding SCFs of both approaches are listed in **Table 3**, while the effect of discretization is studied through calculating the relative differences:

$$\Delta_{\mathrm{m}} = \left|\mathrm{SCF}_{\mathrm{coarse}}/\mathrm{SCF}_{\mathrm{fine}} - 1\right| \tag{39}$$

Table 3 Stress concentration factors for plates regarding both mesh configurations and sensitivity through difference (Δ_m%)

L/a	Mat	Eringen's Nonlocal four-node element			Micropolar four-node element			Micropolar nine-node element		
		coarse	fine	Δ_m%	coarse	fine	Δ_m%	coarse	fine	Δ_m%
3.0	1	1.78606	1.78202	0.23	1.78605	1.78201	0.23	1.73393	1.70319	1.80
	2	1.52022	1.50976	0.69	1.51411	1.50737	0.45	1.48545	1.47719	0.56
	3	1.82143	1.82863	0.39	1.80043	1.79016	0.57	1.73912	1.70772	1.84
	4	1.54508	1.5424	0.17	1.48863	1.48308	0.37	1.46474	1.45855	0.42
10.0	1	1.67799	1.68808	0.60	1.67799	1.68808	0.60	1.64709	1.63256	0.89
	2	1.42931	1.43197	0.19	1.46891	1.47091	0.14	1.44386	1.43921	0.32
	3	1.70709	1.72469	1.02	1.6892	1.69607	0.41	1.64774	1.63248	0.93
	4	1.45055	1.45891	0.57	1.44673	1.4479	0.08	1.42418	1.42011	0.29
20.0	1	1.65415	1.6768	1.35	1.65415	1.6768	1.35	1.6605	1.6143	2.86
	2	1.41681	1.41495	0.13	1.47089	1.46087	0.69	1.44571	1.4315	0.99
	3	1.67154	1.71626	2.61	1.67149	1.68252	0.66	1.66275	1.61416	3.01
	4	1.4289	1.44371	1.03	1.44908	1.43874	0.72	1.42349	1.41348	0.71

Even though second-order elements clearly suppress the first-order ones in problems with high gradients (e.g. stress concentration), the capability of 'explicit' non-local model is studied only in terms of four-node elements. This restriction is a result of excessive computational burden of formation of cross-stiffness matrices (i.e. $\mathbf{k}_{mn}$, $\mathbf{k}_{nm}$) that emerges due to different Jacobians of quadrilateral elements. Hence, for comparison purposes, linear formulation is also implemented to 'implicit' non-local model. According to results listed for Mat (1), it is evident that the solutions are independent from the program used (i.e. COMSOL Multiphysics© and Wolfram Mathematica). To see the global behaviour, the zoom-in and zoom-out looks of contour plots of normal stresses are illustrated at **Figs. 6-7**, together with their variation along vertical axis *y* (see **Fig. 8**). It is worth underlining that since FE method enforces continuity of the displacement field only, the discontinuity of contour maps of the normal stresses among

linear elements were required to be averaged by performing linear interpolation to achieve smooth and physically meaningful stress fields.

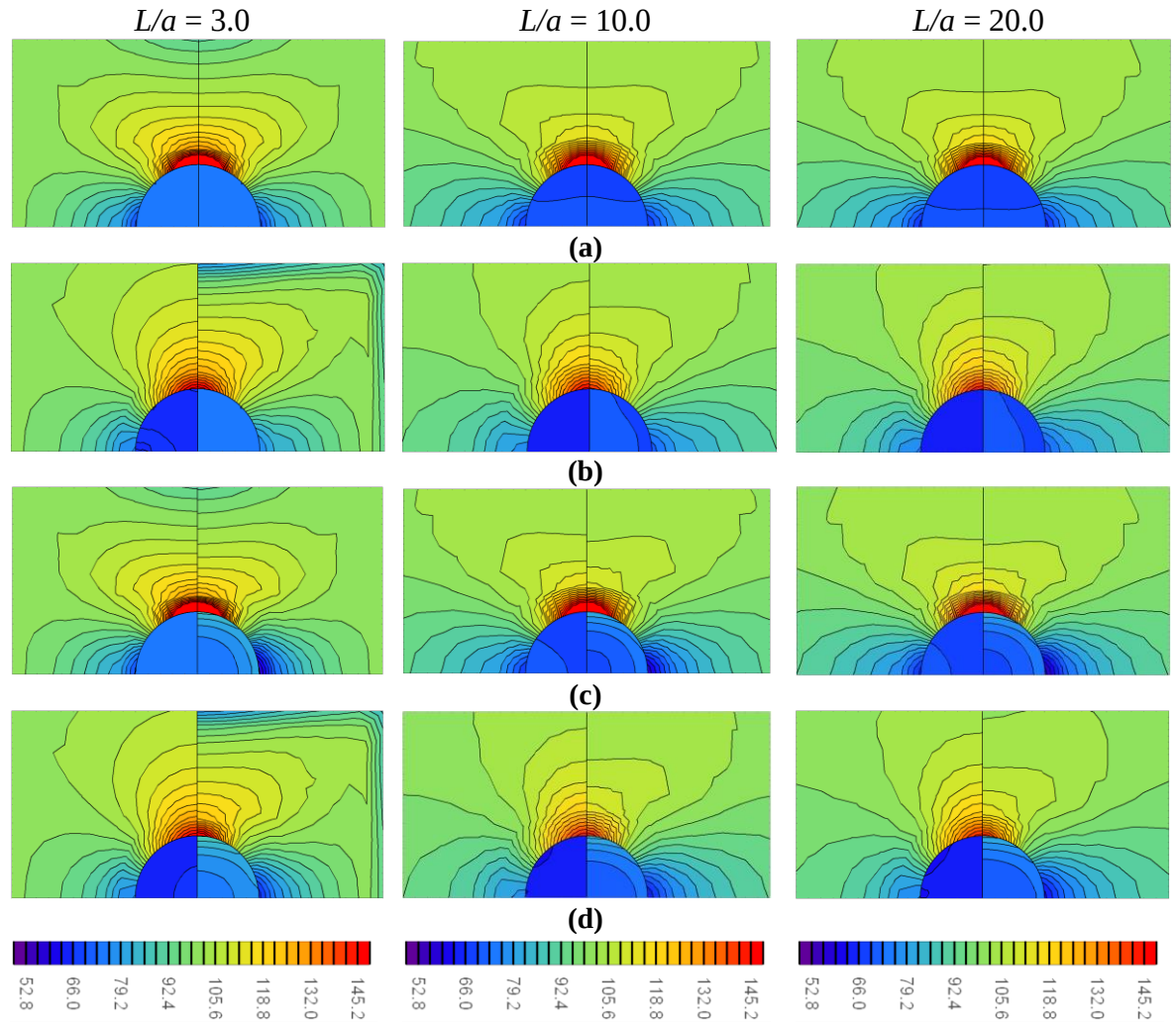

Fig. 6 Zoom-in looks of contour plots of the normal stress field of Cosserat (left) and Eringen (right) non-local four-node, fine meshed FE models for **(a)** Mat (1), **(b)** Mat (2), **(c)** Mat (3), **(d)** Mat (4)

For all scale ratios following inferences can be made independent of the conducted non-local continuum theory:

- As the scale ratio decreases, SCF increases regardless of size effects,

- Having a matrix with size effects leads to decrease in the SCFs (e.g. approximately 14% for Mats (2) and (4)), which highlights the necessity of using a non-classical type theory in such a case,

- The presence of internal length in inclusion seems to have negligible effect on the stress field of matrix region,

- For matrix with size effects, the dependence of SCFs on spatial discretization is weakened compared to Cauchy type matrix. This situation is more evident for second order elements, which may be due to the following reason: Since the error of stresses are known to be minimum

at GQ points, moving away from GQ points would introduce more numerical errors in quadratic elements compared to linear elements of same dimensions due to higher estimation of stress gradients.

The above-mentioned results are in accordance with the existing literature [**32**, **48**]. In the following subsections, the comments about each model with different scale ratios will be detailed with focusing on the conducted non-local theory.

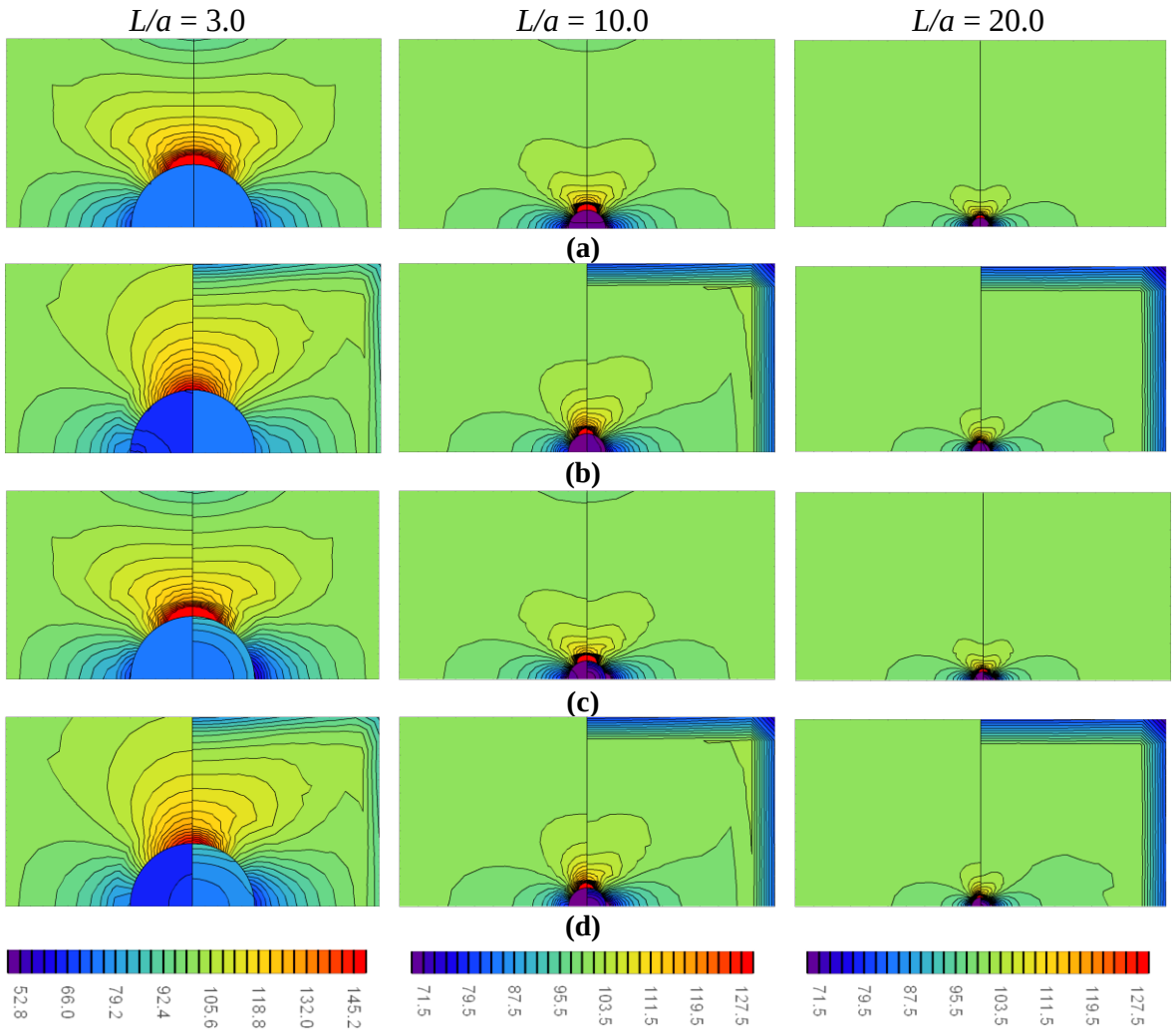

Fig. 7 Zoom-out looks of contour plots of the normal stress field of Cosserat (left) and Eringen (right) non-local four-node, fine meshed FE models for **(a)** Mat (1), **(b)** Mat (2), **(c)** Mat (3), **(d)** Mat (4)

3.1 Plate Model 1 (L/a = 3.0)

As the first step, a plate with scale ratio of L/a = 3.0 is examined. In this particular case, the dimension of inclusion is comparable with the length of the plate which indicates the presence of a more definite non-locality with respect to other scale ratios. According to **Figs. 6-8**, two major differences are encountered between the results of 'explicit' and 'implicit' non-local models:

- An increase of stress close to interface is attained for non-local type inclusion (i.e. Mat (3) and Mat (4)),

- A decrease in stress close to boundaries of the domain is attained for non-local type matrix (i.e. Mat (2) and Mat (4))

when Eringen's nonlocal theory is employed.

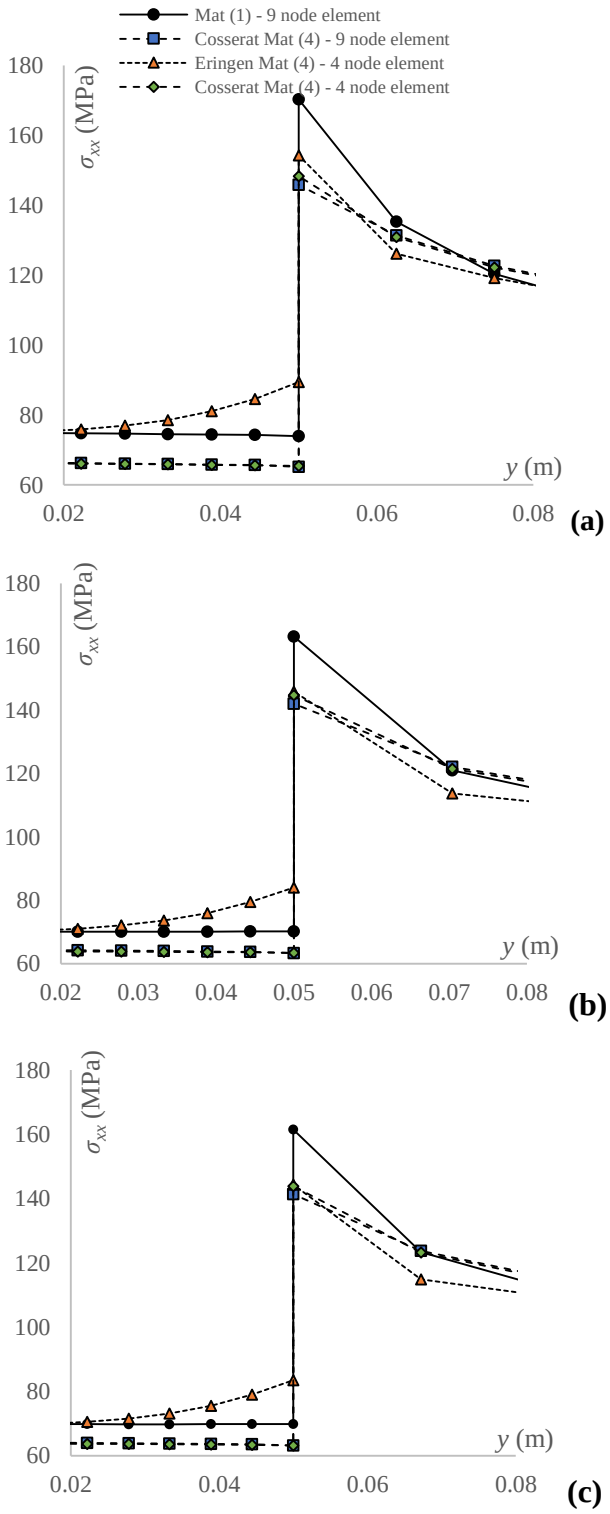

Fig. 8 Normal stress variation along the vertical axis y for **(a)** L/a = 3.0, **(b)** L/a = 10.0, **(c)** L/a = 20.0

Both phenomenon can be explained as a result of 'strong' non-local character of the Eringen model. For the former, the high strain field of matrix around interface, which falls into the influence zone of the inclusion part, results in a rise in stress field of inclusion; while for micropolar theory, such behaviour is not observed. In fact, for micropolar theory, the stress field of inclusion changes depending on the presence of size effects in matrix. One must bear in mind that if an imperfect interface is present, such an interaction between the two regions may weaken or even vanish for both non-local theories. For the latter, the reason of discrepancy seems to be the well-known *boundary effect*, which occurs due to missing contribution of non-existing neighbour elements. It is important to notice that *boundary effects* may be of importance for domains that have dimensions comparable with the influence zone of nonlocal parameter: In order to compensate the decreasing stresses, close to boundaries, the stress at remaining regions needs to be higher due to balance requirement. Indeed, for this particular scale ratio, SCFs of 'explicit' non-local model turns out to be higher than expected for Mats (2) and (4). It is evident if one compares the difference between SCFs of 'implicit' and 'explicit' non-local models regarding all scale ratios: As illustrated in **Fig. 8**., the stresses of both non-local models overlap at point A (i.e. $x = 0$, $y = 0.05$ [m]) except for $L/a = 3.0$, in which case 'explicit' non-local model ends up with a higher estimation of normal stress.

3.2 Plate Model 2 (L/a = 10.0) and Model 3 (L/a = 20.0)

In this section, plates with scale ratios of $L/a = 10.0$ and $L/a = 20.0$ are commented together since no significant difference in terms of stress fields are attained for Models 2 and 3. What is said for $L/a = 3.0$ about 'explicit' and 'implicit' non-local models holds with a slight adjustment: although boundary effects still exist, it has negligible effect around inclusion.

As for $L/a = 20.0$, the plate can be assumed as an infinite medium with a small inclusion, SCFs tabulated in **Table 3** are compared with the analytical values reported in the literature (Atroshchenko et al. [**48**]), by calculating their relative difference (i.e. at point A):

$$\Delta = \left| \frac{\mathrm{SCF}_{\mathrm{numerical}}}{\mathrm{SCF}_{\mathrm{analytical}}} - 1 \right| \tag{40}$$

Comparative results determined via Eq. 40 are listed in **Table 4.** The solutions of both non-local models appear to be in a good agreement with existing literature except for Mat (3): The relative error with respect to the analytical solution tends to increase for both non-local models with linear elements as the mesh is refined. This drawback is suppressed with nine-node elements, and the inherent advantage of using a second-order element formulation in case of

strong material discontinuity is pointed out. Moreover, very similar situation is encountered for Mat (1), which suggests this drawback is stemmed from purely computational issues. Contrarily, for material configurations possessing a non-classical type matrix as in Mat (2) and Mat (4), the results tend to be independent from the spatial discretization (see **Fig. 8**) and tend to converge to explicit solutions for 'implicit' non-local model. Although this seems a bit different for 'explicit' non-local model, the slight increase in error is most likely due to the simplifications made for numerical calculations: number of Gauss Quadrature points and range of influence zone is selected such that the numerical integration with GQ technique provides less than %2 error with respect to numerical integration schemes embedded in Mathematica. Consideration of larger number of GQ points and wider range of influence zone will reduce the errors, but will increase the computational burden dramatically. Note that 'implicit' model formulation does not require any more effort for numerical integration than local elasticity formulation.

Table4. Error (Δ%) with respect to explicit results reported in literature for infinite plates

Mat	Analytical results	Eringen's Nonlocal four-node element		Micropolar four-node element		Micropolar nine-node element	
		coarse	fine	coarse	fine	coarse	fine
1	1.576	4.96	6.40	4.96	6.40	5.36	2.43
2	1.427	0.71	0.84	3.08	2.37	1.31	0.32
3	1.576	6.06	8.90	6.06	6.76	5.50	2.42
4	1.412	1.20	2.25	2.63	1.89	0.81	0.10

5 Conclusion

In the present study, the elasticity problem of a plate with a circular inclusion under uniaxial tensile loading is investigated in terms of both 'implicit'/'weak' and 'explicit'/'strong' non-classical continuum models, Cosserat (micropolar) and Eringen's nonlocal theory, respectively, by employing the finite element method. For both theories, inclusion is incorporated as a heterogeneity possessing different material properties than matrix. The internal characteristic length of Cosserat model is assumed to be known while the non-locality of Eringen's model is tuned via optimizing the value of fraction coefficient in order to be in accordance with the analytical expressions of SCF reported for infinite Cosserat plates. Hence, Eringen's theory is not here used to model solids at atomistic scale, but rather the focus is on structures dominated by other kinds of discrete nature (e.g. heterogeneity) yielding an apparent non-local mechanical behaviour. In this way, apparently for the first time, a comparison between micropolar and Eringen's nonlocal theory of elasticity is performed, both in local and

global manners, in the simplified context of two-dimensional inclusion-matrix problem that possess geometric singularities.

According to the numerical simulations performed for different scale ratios and material configurations, optimization of fraction coefficient of 'explicit' description seem to provide a reasonable approximation to stress concentration factors obtained by 'implicit' theory, in which the peak stresses at the interface are reduced approximately about 14% for non-local type matrix configuration. Such significant decrease in SCFs highlights the necessity of utilizing a non-local type theory in the presence of size effects. On the other hand, major are observed especially at the boundaries of non-local type inclusion and non-local type matrix. This discrepancy is attributed to 'strong' non-local character of Eringen model, that captures the interaction of particles within a neighbourhood which, also, paves the way to modelling the well-known *boundary effect* in atomic simulations.

These observations provide an insight to possible advantages and drawbacks of both non-local descriptions, depending on the application. For instance, if this problem is a sub-model extracted from inner parts of a structure, boundary effects are unlikely to play a role, at least as far as the stress concentration factor is concerned, which justifies the use of 'implicit' description. On the other hand, to examine possible inclusions close to boundaries by sub-modelling, it is apparent that *boundary effects* may alter the stress concentration, and, in the end, the ultimate strength of the structure. In that case, 'explicit' model seems to be the better option. However, the computational burden introduced by 'explicit' modelling, both due to cross-stiffness matrices and numerical integration, should not be underestimated. This naturally brings into consideration using a coupled non-local modelling in which the interior of the domain is modelled by 'implicit' approximation while the boundaries are modelled by 'explicit' description when necessary, by suitable displacement and traction conditions. This may be the next step once a correspondence between two different non-local descriptions are put into evidence.

The numerical examples presented herein can be considered as a first evolution for matrix-inclusion problem, while more rigorous treatment may be required for a better approximation to the actual physical phenomena. For instance, in further studies inclusion and matrix parts can be considered as separate regions, with enforcing some contact constrains for interfacial relation. In that case, the Euclidian distance appeared in kernel function of Eringen's nonlocal model cannot be taken equal to spatial distance, which will yield different results from those currently obtained. In any case, a connection between two different descriptions of non-locality has been demonstrated quantitatively, which is expected to pave the way to more enhanced

modelling of the structures with size effects by unifying the superior aspects of these approaches both theoretically and computationally. To look for deeper correspondences, comparison between both non-local theories are going to be extended to problems that possess load singularities by focusing on both displacement and stress fields.

Acknowledgements This work was done when Meral Tuna was a Visiting Researcher at DISG, Sapienza University of Rome, with financial support of Italian Ministry of University and Research PRIN 2015, project 2015JW9NJT (Grant No. B86J16002300001, ID: 10.13039/501100003407) "Materials with microstructure: multiscale models for the derivation non-local continua of 'implicit/weak' and explicit/strong'" which is gratefully acknowledged.

Conflict of interest The authors have no conflict of interest to report.

References

1. de Borst R (1991) Simulation of strain localization: A reappraisal of the Cosserat continuum. Eng Comput 8:317-332

2. Sluys LJ, de Borst R, Mühlhaus HB (1993) Wave propagation, localization and dispersion in a gradient-dependent medium. Int J Solid Struct 30:1153-1171

3. Zhang X, Sharma P (2005) Inclusions and inhomogeneities in strain gradient elasticity with couple stress and related problems. Int J Solid Struct 42:3833-3851

4. Trovalusci P, Pau A (2014) Derivation of microstructured continua from lattice systems via principle of virtual works. The case of masonry-like materials as micropolar, second gradient and classical continua. Acta Mech 225:157-177

5. Trovalusci P (2016) Discrete to Scale-Dependent Continua for Complex Materials. A Generalized Voigt Approach Using the Virtual Power Equivalence. In: Trovalusci P (ed) Materials with Internal Structure. Multiscale and Multifield Modelling and Simulation, Springer Tracts in Mechanical Engineering Series, 1st edn. Springer International Publishing, Switzerland, pp 109-131

6. Suzuki T, Takeuchi S, Yoshinaga H (1991) Dislocation Dynamics and Plasticity. Springer-Verlag, Berlin

7. Rapaport DC, Rapaport DCR (2004) The art of Molecular Dynamics simulation. Cambridge University Press, Cambridge

8. Yang D, Sheng Y, Ye J, Tan Y (2010) Discrete element modelling of the microbond test of finer reinforced composite. Comput Mater Sci 49:253-259

9. Godio M, Stefanou I, Sab K, Sulem J, Sakji S (2017) A limit analysis approach based on Cosserat continuum for the evaluation of the in-plane strength of discrete media: application to masonry. Eur J Mech A Solids 66:168-192

10. Reccia E, Leonetti L, Trovalusci P, Cecchi A (2018) A multiscale/multidomain model for the failure analysis of masonry walls: a validation with a combined FEM/DEM approach. Int J Mult Comp Eng 16:325-343

11. Mindlin RD (1965) Second gradient of strain and surface-tension in linear elasticity. Int J Solid Struct 1:417-438

12. Capriz G (1989) Continua with Microstructure. Springer-Verlag, New York

13. Maugin A (1993) Material Inhomogenities in Elasticity. Chapman and Hall, London

14. Eringen AC (1999) Microcontinuum Field Theories. Springer-Verlag, New York

15. Gurtin ME (1999) Configurational Forces as Basis Concept of Continuum Physics. Springer-Verlag, New York

16. Eringen AC (2002) Nonlocal Continuum Field Theories. Springer-Verlag, New York.

17. Cosserat E, Cosserat F (1896) Sur la theorie de l'elasticite. Ann. de l'Ecole Normale de Toulouse 10:I1-I116

18. Eringen AC (1966) Linear theory of micropolar elasticity. J Math Mech 15:909-923.

19. Nowacki W (1986) Theory of Asymmetric Elasticity. Pergamon, New York.

20. Eringen AC, Edelen DGB (1972) On nonlocal elasticity. Int J Eng Sci 10:233-148

21. Eringen AC (1974) Theory of nonlocal thermoelasticity. Int J Eng Sci 12:1063-1077

22. Kunin IA (1968) The Theory of Elastic Media with Microstructure and the Theory of Dislocations. In: Kröner E (ed) Mechanics of Generalized Continua, 1st edn. Springer-Verlag, Berlin Heidelberg, pp 321-329

23. Kunin IA (1984) On foundations of the theory of elastic media with microstructure. Int J Eng Sci 22:969-978

24. Chen Y, Lee JD (2004) Atomistic viewpoint of the applicability of microcontinuum theories. Int J Solid Struct 41:2085-2097

25. Trovalusci P (2014) Molecular Approaches for Multifield Continua: Origins and Current Developments. In: Sadowski T, Trovalusci P (ed) Multiscale Modeling of Complex Materials: Phenomenological, Theoretical and Computational Aspects, CISM International Centre for Mechanical Sciences Series, 1st edn. Springer-Verlag, Wien, pp 211-278

26. Masiani R, Trovalusci P (1996) Cosserat and Cauchy materials as continuum models of brick masonry. Meccanica 31:421-432

27. Forest S, Sab K (1998) Cosserat overall modeling of heterogeneous materials. Mech Res Commun 25:449-454

28. Forest S, Dendievel R, Canova GR (1999) Estimating the overall properties of heterogeneous Cosserat materials. Model Simul Mater Sci Eng 7:829–840

29. Pau A, Trovalusci P (2012) Block masonry as equivalent micropolar continua: the role of relative rotations. Acta Mech 223:1455-1471.

30. Trovalusci P, De Bellis ML, Masiani R (2017) A multiscale description of particle composites: From lattice microstructures to micropolar continua. Compos Part B-Eng 128:164-173

31. Leonetti L, Greco F, Trovalusci P, Luciano R, Masiani R (2017) A multiscale damage analysis of periodic composites using a couple-stress/Cauchy multidomain model: Application to masonry structures. Compos Part B-Eng 118:75-95

32. Fantuzzi, N, Leonetti, L, Trovalusci P, Tornabene, F (2018) Some novel numerical applications of Cosserat continua. Int J Comput Methods 15:1850054-1-38

33. Fantuzzi N, Trovalusci P, Dharasura S (2019) Mechanical behaviour of anisotropic composite materials as micropolar continua. Frontiers 59:1-11

34. Kröner E (1967) Elasticity theory of materials with long range cohesive forces. Int J Solid Struct 3:731-742

35. Krumhansl J (1968) Some Considerations of the Relation Between Solid State Physics and Generalized Continuum Mechanics. In: Kröner E (ed) Mechanics of Generalized Continua, xx edn. Springer-Verlag, Berlin Heidelberg, pp 298-311

36. Eringen AC (1966) A unified theory of thermomechanical materials. Int J Solid Struct 4:179-202

37. Eringen AC (1972) Linear theory of nonlocal elasticity and dispersion of plane waves. Int J Eng Sci 10:425-435

38. Eringen AC (1983) On differential equations of nonlocal elasticity and solutions of screw dislocation and surface waves. J Appl Phys 54:4703-4710

39. Polizzotto C, Fuschi P, Pisano AA (2006) A nonhomogenous nonlocal elasticity model. Eur J Mech A-Solid 25:308-333

40. Hosseini M, Hadi A, Malekshahi A, Shishesaz M (2018) A review of size-dependent elasticity for nanostructures, Jcamech 49:197-211

41. Tuna M, Kirca M, Trovalusci P (2019) Deformation of atomic models and their equivalent continuum counterparts using Eringen's two-phase local/nonlocal model. Mech Res Commun 97: 26-32

42. Sadowski T (2014) Modelling of damage and fracture process of ceramic matrix composites under mechanical loading. In: Sadowski T, Trovalusci P (ed) Multiscale Modeling of Complex Materials: Phenomenological, Theoretical and Computational Aspects, CISM International Centre for Mechanical Sciences Series, 1st edn. Springer-Verlag, Wien, pp 211-278

43. Hubert D, Sadowski T (2017) Modelling of the damage process of interfaces inside the WC/Co composite microstructure: 2-D versus 3-D modelling technique. Compos Struct 159:121-127.

44. Postek E, Sadowski T (2019) Impact model of WC/Co composite. Compos Struct 213:231-242.

45. Lubarda VA (2003) Circular inclusions in anti-plane strain couple stress elasticity. Int J Solid Struct 40:3827-3851

46. Zhang X, Sharma P (2005) Inclusion and inhomogeneities in strain gradient elasticity with couple stresses and related problems. Int J Solid Struct 42:3833-3851

47. Dong H, Wang J, Rubin MB (2014) Cosserat interphase models for elasticity with application to the interphase bonding a spherical inclusion to an infinite matrix. Int J Solid Struct 51:462-447

48. Atroshchenko E, Hale JS, Videla JA, Potapenko S, Bordas SPA (2017) Micro-structures materials: Inhomogeneties and imperfect interfaces in plane micropolar elasticity, a boundary element approach. Eng Anal Bound Elem 83:195-203

49. Polizzotto C (2001) Nonlocal elasticity and variational principles. Int J Solid Struct 38:7359-7380

50. Pisano AA, Sofi A, Fuschi P (2009) Nonlocal integral elasticity: 2D finite element based solutions. Int J Solid Struct 46:3836-3849

51. Pisano AA, Sofi A, Fuschi P (2009) Finite element solutions for nonhomogeneous nonlocal elastic problems. Mech Res Commun 36:755-761

52. Fuschi P, Pisano AA, De Domenica D (2015) Plane stress problems in nonlocal elasticity: finite element solutions with a strain-difference-based formulation. J Math Anal Appl 431:714

53. Pisano AA, Fuschi P (2018) Stress evaluation in displacement-based 2D nonlocal finite element method. Curved and Layered Structures 5:136-145

54. COMSOL Multiphysics® v. 5.2. COMSOL AB, Stockholm, Sweden. 2015.

55. Mathematica, version 11.3 Wolfram Research, Inc., Champaign, IL 2018.

56. Sokolowski M (1972) Theory of couple stresses in bodies with constrained rotations. Springer, Wien

57. Lakes RS (1995) Experimental methods for study of Cosserat elastic solids and other generalized continua. In: Mühlhaus H (ed) Continuum Models for materials with Micro-Structure, 1st edn. John Wiley, New York, pp 1-22

58. Trovalusci P, Masiani R (1999) Material symmetries of micropolar continua equivalent to lattices. Int J Solid Struct 36:2091-2108

59. Marotti de Sciarra F (2009) On non-local and non-homogenous elastic continua. Int J Solid Struct 46:651-676

60. Ghosh S, Sundararaghavan V, Waas AM (2014) Construction of multi-dimensional isotropic kernels for nonlocal elasticity based on phonon dispersion data. Int J Solid Struct 51:392-401

61. Faroughi SH, Goushegir SMH, Khodaparast HH, Friswell MI (2017) Nonlocal elasticity in plates using novel trial functions. Int J Mech Sci 130:221-233

62. Khodabakhshi P, Reddy JN (2015) A unified integro-differential nonlocal model. Int J Eng Sci 95:60-75

63. Pisano AA, Fuschi P (2018) Structural symmetry and boundary conditions for nonlocal symmetrical problems. Meccanica 53:629-638

64. Storn R, Price K (1997) Differential Evolution – A simple and efficient heuristic for global optimization over continuous spaces. J Global Optim 11:341-359